

All-optical digital logical system based on unidirectional modes

Jie Xu^{1,2}, Yamei Luo^{1,2}, Sanshui Xiao³, Fengwen Kang^{3,4,5}, and Kosmas L. Tsakmakidis⁶

¹*School of Medical Information and Engineering,
Southwest Medical University, Luzhou 646000, China*

²*Medical Engineering & Medical Informatics Integration and
Transformational Medicine of Luzhou Key Laboratory, Luzhou 646000, China*

³*DTU Fotonik, Department of Photonics Engineering,
Technical University of Denmark, DK-2800 Kgs. Lyngby, Denmark*

⁴*Laboratory of Advanced Nano Materials and Devices,
Ningbo Institute of Materials Technology and Engineering (NIMTE),
Chinese Academy of Sciences (CAS), Ningbo, 315201, China*

⁵*College of Materials Science and Engineering,
Sichuan University, Chengdu 610065, China*

⁶*Section of Condensed Matter Physics, Department of Physics,
National and Kapodistrian University of Athens,
Panepistimioupolis, GR-157 84 Athens, Greece and
Corresponding authors: K. L. Tsakmakidis (ktsakmakidis@phys.uoa.gr),
J. Xu (xujie011451@163.com), and F. Kang (kangfengwen0597@126.com)*

Abstract

Standard electronic computing based on nanoelectronics and logic gates has upended our lives in a profound way. However, suffering from, both, Moore's law and Joule's law, further development of logic devices based solely on electricity has gradually stuck in the mire. All-optical logic devices are believed to be a potential solution for such a problem. In this paper, we propose an all-optical digital logical system (AODLS) based on unidirectional (one-way propagation) modes in the microwave regime. In a Y-shaped module of the AODLS, the basic seven logic gates, including OR, AND, NOT, NOR, NAND, XOR, and XNOR gates, are achieved for continuous broadband operation relying on the existence of unidirectional electromagnetic (EM) signals. Extremely large extinction and contrast ratios are found in these logic gates. The idea of 'negative logic' is used in designing the AODLS. Moreover, we further demonstrate that the AODLS can be assembled to multi-input and/or multi-output logical functionalities, which is promising for parallel computation. Besides, numerical simulations perfectly fit with and corroborate our theoretical analyses. The low-loss, broadband, and robust characteristics of this system are outlined and studied in some detail. The AODLS consisting of unidirectional structures may open a new route for all-optical calculation and integrated optical circuits.

I. INTRODUCTION

Moore's law has indicated and underlined the direction for the development of electrical communication for almost fifty years now. To achieve even faster communications with less energy consumption and smaller devices, a new generation of devices is needed. Optical communication, owing to its ultra-fast data transmission, immune to cross-talk[1, 2] and minimal or even zero[3] energy loss, is believed to be a promising candidate.

In 1969, S. E. Miller proposed 'Integrated Optics' for the first time[4]. Since then, massive attempts have been made on integrated optical circuits (IOCs), the analog of the integrated electrical circuit. At present, many kinds of optical logic gates (LGs), one of the basic elements of the IOC, have been achieved in micro-ring resonators[5–8], Mach-Zehnder interferometers[9–11], plasmonic nanostructures[12–15], photonic crystals (PhCs)[16–19], microcavities[20, 21], magnetic[22, 23] or two-dimentional (2D) material-based systems[24–27]. Notably, the quantum LGs[28–30] are another potential way to the next generation communications, and in this work, we only focus on the classic all-optical LGs.

The aforementioned all-optical LGs are limited by one or more following conditions: 1) the discrete and/or narrow operating band[31], 2) different input-output frequencies ($f_{\text{in}} \neq f_{\text{out}}$)[6, 32], 3) the complex fabrication processes, and 4) relatively low signal-to-noise ratio. Besides, the logic states in the above LGs are dependent on the input-output energy intensities, or the polarizations/phase or DC potential, resulting in the low extinction ratio (ER) and contrast ratio (CR) between logic "0" and logic "1". To our knowledge, the ER and CR in the previously reported works are usually below 30 dB[33]. We emphasize here that R. Agarwal's group has theoretically proposed a one-dimensional system that could achieve the logic operations with $\text{ER} \approx 100$ dB. However, limited by the precise manufacturing process, they only achieved the XOR gate with $\text{ER} \approx 20$ dB[19]. To a certain extent, the values of the ER and CR could be enlarged by improving the manufacturing process or the monitoring technology; however, the error rate (E_r) will remain more or less the same. To achieve ultra-high-performance optical communication, precise logic states are required, and in this work, we shall show that the unidirectional mode-based devices have the potential for achieving this goal.

Unidirectional (one-way) modes are those electromagnetic (EM) modes that are allowed to propagate only in one direction. They can be attained in several different structures, for example, the magneto-optical (MO) heterostructures[34–38], topological metamaterial[39], and topological photonic crystals (PhCs)[40, 41]. The MO heterostructures, without doubt, are technically the most simple way to build one-way waveguides. The robust one-way propagating EM waves without backscattering have been observed in the laboratory by designing nonreciprocal MO PhCs[42]. In 2017, we found that owing to the one-way property, the MO heterostructure terminated by metal layers could overcome the time-bandwidth limit because of the broken Lorentz reciprocity[35]. Recently, we have proposed several MO one-way waveguides in which interesting functionalities such as slow light[34, 43], bidirectionally rainbow trapping and releasing[44], and true rainbow trapping[36, 45] were achieved. The one-way propagation characteristic is very suitable and desired for designing LGs because the one-way modes are insensitive to disorders and bends[46, 47], and the noise barely exists in such devices. However,

how to assemble one-way structures flexibly and make them work as multiple LGs is currently an ongoing progress [48].

In this paper, we propose the LGs and the all-optical digital logical system (AODLS) based on robust unidirectional modes. In the AODLS, the ER and CR are founded to diverge in theory, while the error rate (Er) is negligible. Applying the logical and negative logical concepts, multiple LGs are achieved in a single Y-shaped module of the AODLS for the whole relatively broad one-way band. More interestingly, besides the advantages of the enormous ER and CR and incredibly small Er , the unidirectional-modes based AODLS could be used in parallel operation[49] with multiple inputs and/or outputs due to its expandability. This work aims to point out a new path for all-optical calculations, with the simple universal AODLS being easily extendable to other higher regimes.

II. THE Y-SHAPED MODULE OF THE AODLS

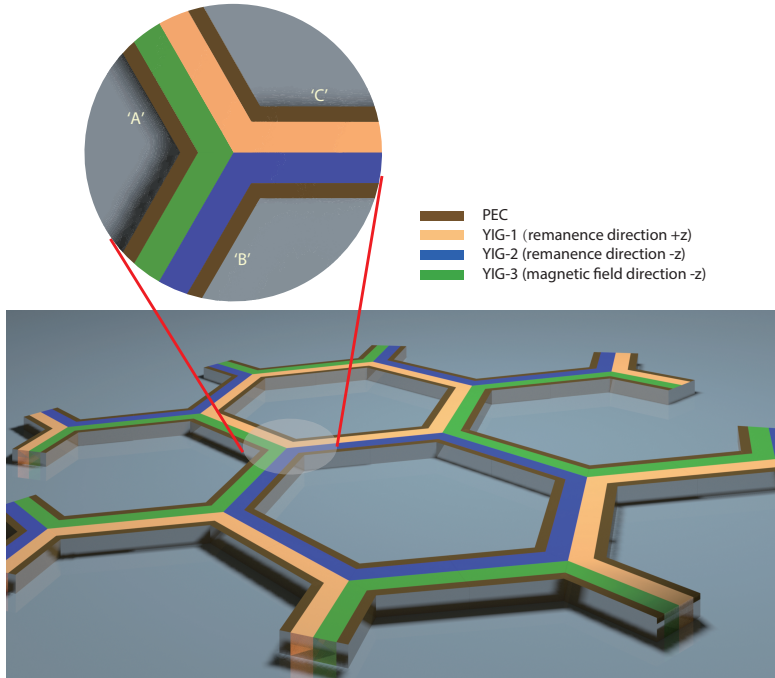


FIG. 1. The schematic of the all-optical digital logical system (AODLS). The yellow, blue and green colored materials represent YIG-1 with remanence ($+z$), YIG-2 with remanence ($-z$) and YIG-3 under an EMF ($-z$).

In this subsection, we first study the propagation characteristics in the basic module of the AODLS. The schematic of the AODLS is shown in Fig. 1. As one can see, the system is constructed by three basic elements/arms, i.e. 'A', 'B' and 'C', which are built by three types of magnetized yttrium-iron-garnet (YIG) materials. The yellow and blue colored materials represent the YIG with remanence, and the magnetization directions are $+z$ and $-z$, respectively. The last kind of the YIG layer is magnetized by an external magnetic field (EMF) B_0 ($-z$). For simplicity, the above YIG layers are named YIG-1, YIG-2 and YIG-3, respectively. The zoom-in

picture in Fig. 1 shows one of the basic Y-shaped modules of the AODLS. To clearly illustrate how the module works for logic operations, we investigate the propagation characteristics of the guiding modes in the arms 'A', 'B' and 'C'. Due to the existence of the magnetization, the relative permeability of YIG-1, YIG-2 and YIG-3 respectively takes the following forms

$$\bar{\mu}_{r1} = \begin{bmatrix} \mu_{1r} & i\mu_{2r} & 0 \\ -i\mu_{2r} & \mu_{1r} & 0 \\ 0 & 0 & 1 \end{bmatrix} \quad \bar{\mu}_{r2} = \begin{bmatrix} \mu_{1r} & -i\mu_{2r} & 0 \\ i\mu_{2r} & \mu_{1r} & 0 \\ 0 & 0 & 1 \end{bmatrix} \quad \bar{\mu} = \begin{bmatrix} \mu_1 & -i\mu_2 & 0 \\ i\mu_2 & \mu_1 & 0 \\ 0 & 0 & 1 \end{bmatrix} \quad (1)$$

where $\mu_{1r} = 1$, $\mu_{2r} = -\frac{\omega_r}{\omega}$, $\mu_1 = 1 + \frac{\omega_m \omega_0}{\omega_0^2 - \omega^2}$ and $\mu_2 = \frac{\omega_m \omega}{\omega_0^2 - \omega^2}$ [50, 51]. $\omega_0 = 2\pi\gamma B_0$ is the precession angular frequency, and $\omega_r = 2\pi \times 3.587 \times 10^9$ rad/s is the characteristic circular frequency[52]. According to the Maxwell's equations and the boundary conditions, one can easily calculate the dispersion equations in the above three 'arms', and the equations are wrotten as follow

$$\frac{\mu_{2r}}{\mu_{1r}}k + \frac{\alpha_1}{\tanh(\alpha_1 d)} + \frac{\mu_{vr}}{\mu_v} \left[\frac{\mu_2}{\mu_1}k + \frac{\alpha}{\tanh(\alpha d)} \right] = 0 \quad ('A') \quad (2)$$

$$\frac{-\mu_{2r}}{\mu_{1r}}k + \frac{\alpha_1}{\tanh(\alpha_1 d)} + \frac{\mu_{vr}}{\mu_v} \left[\frac{\mu_2}{\mu_1}k + \frac{\alpha}{\tanh(\alpha d)} \right] = 0 \quad ('B') \quad (3)$$

$$\frac{\mu_{2r}}{\mu_{1r}}k + \frac{\alpha_1}{\tanh(\alpha_1 d)} = 0 \quad ('C') \quad (4)$$

where α_1 and α are the attenuation coefficients of the surface magnetoplasmons (SMPs) in the YIG-1/2 and YIG-3. The complete one-way propagation (COWP) bands are characterized by the asymptotic frequencies (AFs), and deriving from Eqs. (2)-(4), we find that

$$\begin{aligned} \omega_{AF_P1} &= \omega_r \\ \omega_{AF_P2} &= \omega_0 + \omega_m \\ \omega_{AF_N1} &= \frac{2\omega_0 + \omega_m + \omega_r - \sqrt{(2\omega_0 + \omega_m + \omega_r)^2 - 8\omega_0\omega_r}}{4} \\ \omega_{AF_N2} &= \frac{2\omega_0 + \omega_m + \omega_r + \sqrt{(2\omega_0 + \omega_m + \omega_r)^2 - 8\omega_0\omega_r}}{4} \end{aligned} \quad (5)$$

for 'A', and

$$\begin{aligned} \omega_{AF_P1} &= \frac{-(2\omega_0 + \omega_m - \omega_r) + \sqrt{(2\omega_0 + \omega_m - \omega_r)^2 + 8\omega_0\omega_r}}{4} \\ \omega_{AF_P2} &= \omega_0 + \omega_m \\ \omega_{AF_N1} &= \omega_r \end{aligned} \quad (6)$$

$$\omega_{AF_N2} = \frac{2\omega_0 + \omega_m - \omega_r + \sqrt{(2\omega_0 + \omega_m - \omega_r)^2 + 8\omega_0\omega_r}}{4}$$

for 'B', and

$$\omega_{AF_P} = \omega_r \quad (7)$$

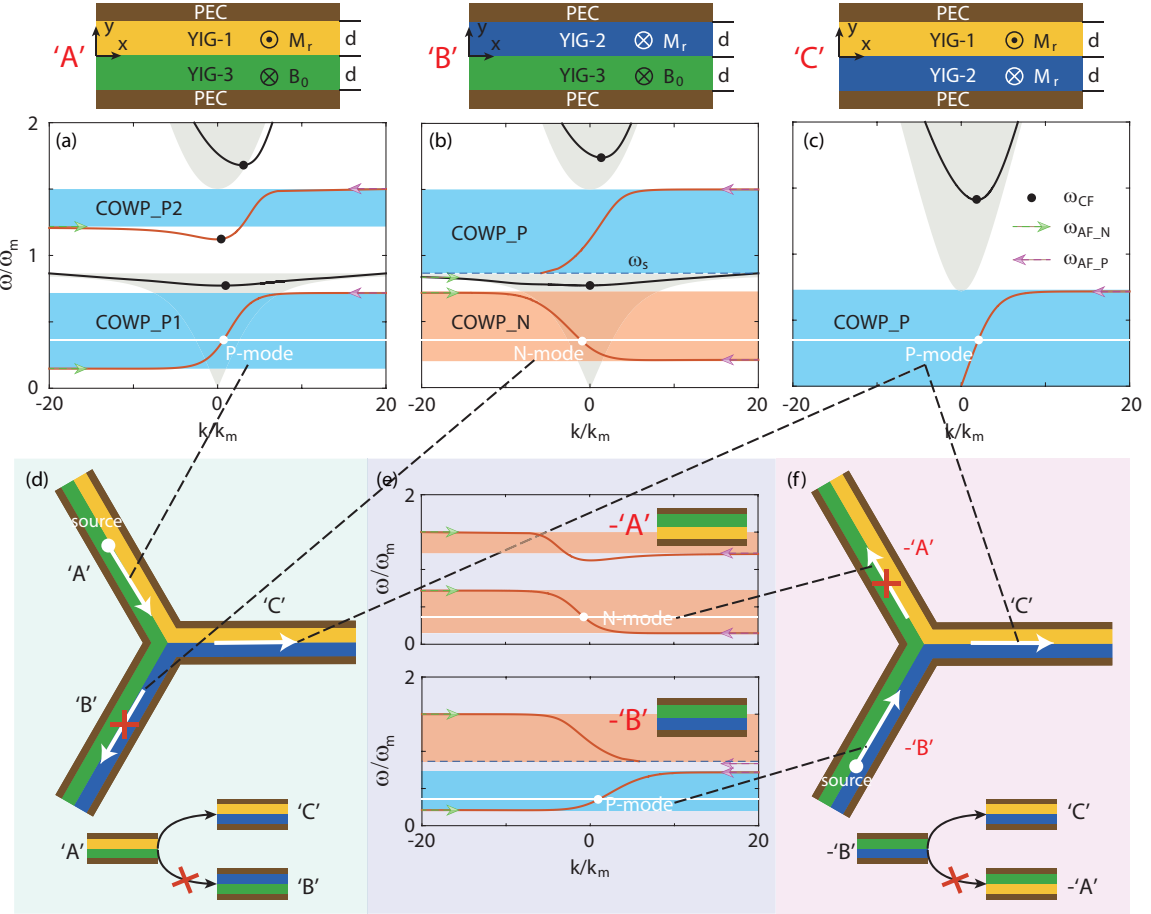


FIG. 2. The dispersion diagram of three arms, i.e. (a) 'A', (b) 'B', and (c) 'C', of the Y-shaped logical module. The red and black lines indicate the surface modes and lowest-order bulk modes, respectively. The other parameters are $\omega_0 = 0.5\omega_m$, $d = 0.05\lambda_m$ and $\omega_r = 2\pi \times 3.587 \times 10^9$ rad/s. (d,f) Two one-way channels in the Y-shaped module. (e) The dispersion diagram of the arms '-A' and '-B'.

for 'C'. We note here that ω_{AF_P} and ω_{AF_N} are the AFs for $k \rightarrow +\infty$ and $k \rightarrow -\infty$, respectively. It is clear that the three arms possess one same AF, i.e. $\omega_{AF} = \omega_r$, which is the only AF in the arm 'C' while the other arms have two additional AFs. To further explore the dispersion relations in the arms, we plotted the dispersion diagram for $\omega_0 = 0.5\omega_m$ ($\omega_m = 10\pi \times 10^9$ rad/s, the characteristic circular frequency) and $d = 0.05\lambda_m$ ($\lambda_m = 2\pi c/\omega_m$). In this case, as shown in Fig. 2(a), there are two COWP regions in the arm 'A', and four AFs (marked by arrows) are observed as well.

Moreover, the waves in both COWP regions can only propagate in the same direction, i.e. $+x$ direction. Similarly, two COWP bands are found in the arm 'B' (see Fig. 2(b)) whereas the SMPs in the lower COWP_N band with the opposite propagation direction, i.e. $-x$ direction. Furthermore, only one COWP_P band is observed in the arm 'C' (see Fig. 2(c)). The COWP bands in the three structures are $0.1482\omega_m < \omega < 0.7174\omega_m$ (COWP_P1) and $1.2105\omega_m < \omega < 1.5\omega_m$ (COWP_P2) for the arm 'A', $0.2105\omega_m < \omega < 0.7174\omega_m$ (COWP_N) and $0.8660\omega_m < \omega < 1.5\omega_m$ (COWP_P) for the arm 'B', and $0 < \omega < 0.7174\omega_m$ (COWP_P) for the arm 'C'. Notably, the lower limit of the COWP_P band in the arm 'B' is not ω_{AF_N2} because it is less than $\omega_s (= \sqrt{\omega_0(\omega_0 + \omega_m)})$ that indicates the edge of the lower bulk zone. It is quite interesting that the COWP bands of the SMPs in the three arms overlap with each

other in some regions, for example, $0.2105\omega_m < \omega < 0.7174\omega_m$ region. Nevertheless, as shown in Fig. 2(d), the guiding waves ('P-mode') within the overlapped band in the arm 'A' of the Y-shaped module can not couple to the opposite modes ('N-mode') in the arm 'B' but can propagate to the arm 'C' due to the robust one-way propagation property. Similarly, there is another one-way channel between the arms 'B' and 'C'. As shown in Figs. 2(e,f), the arm 'B' is equivalent to the arm -'B' in which the EM waves within the overlapped band have positive group velocities. Because of the symmetry, the arm -'A' in this case can only sustain the 'N-mode' (see Fig. 2(e)). In short, the waves in the arms 'A'(-'A') and 'B'(-'B') can only propagate towards the joint of the module while the waves in the output arm 'C' always depart from the joint, constructing two independent one-way channels. Besides, for $1.2105\omega_m < \omega < 1.409\omega_m$, the corresponding guiding waves in the arm 'A' can only travel to the arm 'B' since there are no EM modes in the arm 'C'. The black points in Fig. 2 indicate the cut-off frequencies (ω_{CF}) of the SMPs and the bulk modes, which may affect the boundaries of the COWP bands.

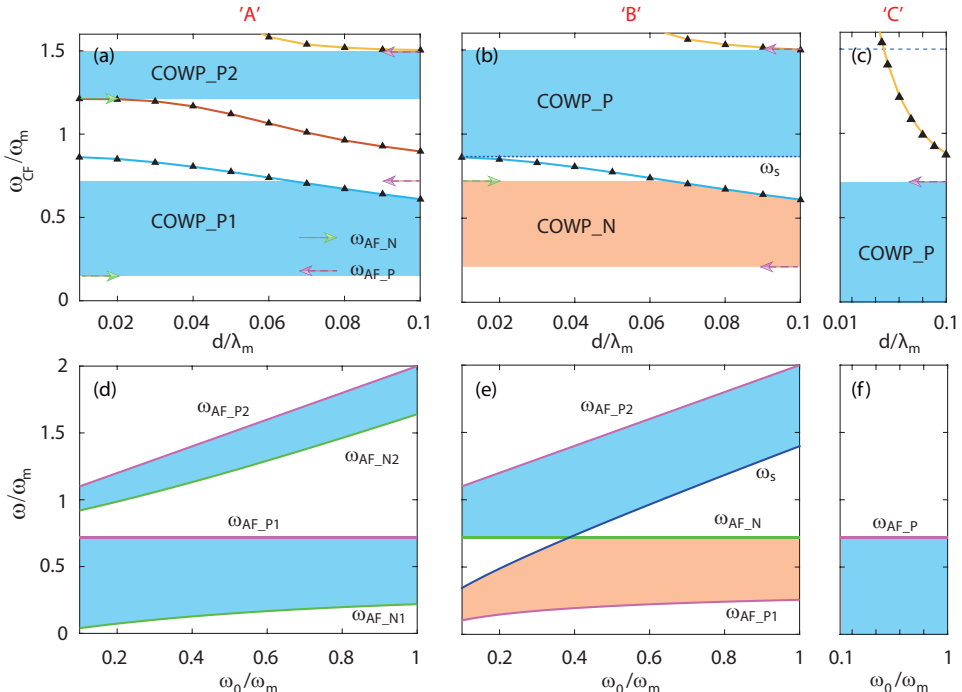


FIG. 3. The cut-off frequencies (marked by black points in Fig. 2) as a function of the thickness parameter in the arms (a) 'A', (b) 'B', and (c) 'C'. (d)-(f) The limits of the COWP bands as a function of ω_0 in the arms 'A', 'B', and 'C'.

In order to further explore the broad COWP band, we studied the correlation between d and ω_{CF} in Figs. 3(a)-(c) as $\omega_c = 0.5\omega_m$. As a result, the COWP bands in the arms 'A', 'B' and 'C' remain almost the same for thin cases, while for $d > 0.067\lambda_m$, the lower COWP bands in the arms 'A' and 'B' become narrow because of the drop-down bulk modes. Moreover, according to our calculation, we found that $\omega_{CF} > 1.5\omega_m$ as $d < 0.047\lambda_m$. Furthermore, we plot AFs and ω_s as a function of ω_0 as $d = 0.05\lambda_m$ to demonstrate the impact of the EMF on the COWP bands. As demonstrated in Fig. 3(d), the COWP_P1 gradually narrows down when enlarging B_0 while the COWP_P2 is slightly widened when enhancing the EMF in the arm 'A'. Complicated change of the COWP bands is observed in Fig. 3(e), in which the maximal total bandwidth of the COWP bands in the arm 'B' occurs around $\omega = 0.4\omega_m$. Additionally,

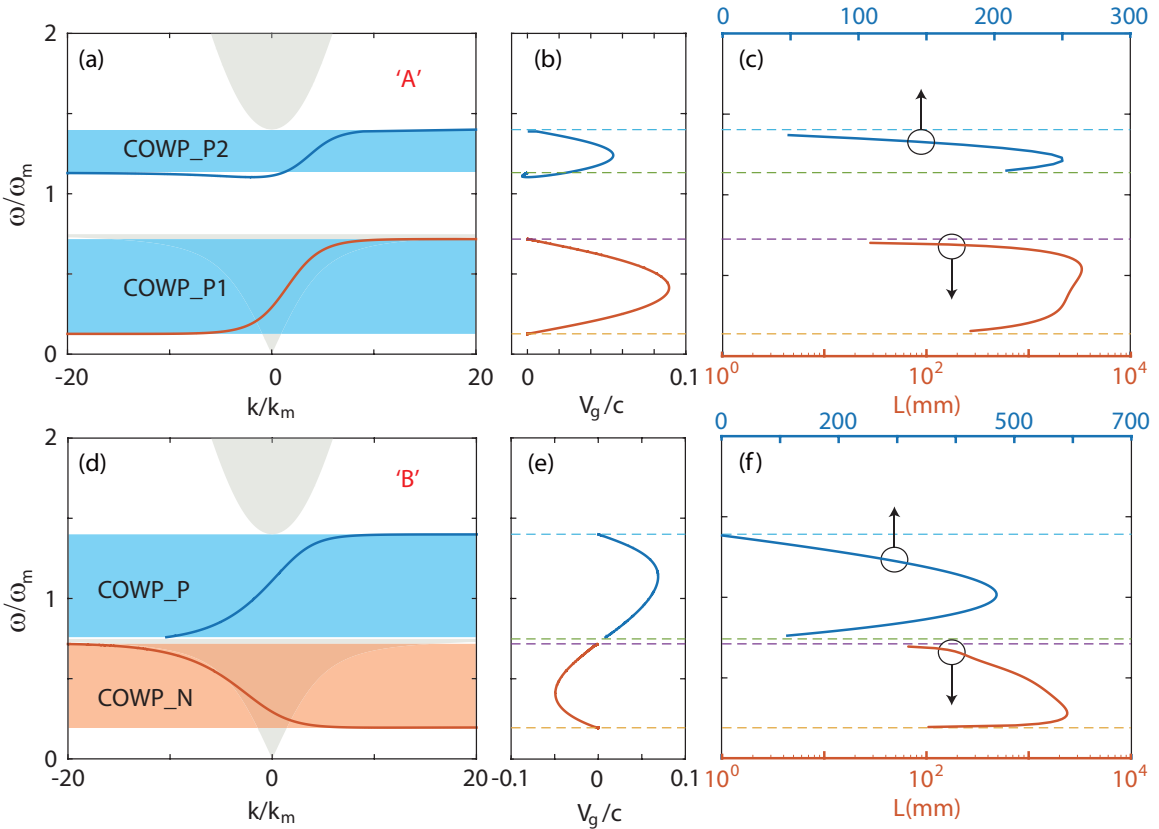


FIG. 4. The dispersion diagrams of (a) the EYYE-r and (d) the EYYE-s configurations as $d = 0.04\lambda_m$ and $\omega_0 = 0.4\omega_m$. (b,e) The group velocities and (c,f) the propagation distances of the one-way modes in the COWP regions. In the lossy cases, the relaxation angular frequency $\nu = 10^{-3}\omega$.

the one-way region of the arm 'C', different from the arms 'A' and 'B', remains unchanged (see Fig. 3(f)) regardless of the EMF because this arm only contains the YIG with remanence. To achieve the broadband optical logic operation based on unidirectional modes, relatively broad COWP bands are required. Thus, according to the above analyses, we choose $d = 0.04\lambda_m$ and $\omega_c = 0.4\omega_m$ in designing the AODLS in the following work. We note that there are multiple band gaps in the dispersion diagrams of the SMPs, which should have further interesting uses in optical isolators and switches. In this work, however, we just focus on the unidirectional modes and their related applications in the logic gates (LGs) and logic operations.

Similar to Figs. 2(a,b), Figs. 4(a,d) shows the dispersion diagrams of the arms 'A' and 'B' as $d = 0.04\lambda_m$ and $\omega_0 = 0.4\omega_m$, and the bandwidths of the COWP bands in the arms 'A' and 'B' are respectively $0.5906\omega_m$ (COWP_P1, $0.1268\omega_m < \omega < 0.7174\omega_m$), $0.2681\omega_m$ (COWP_P2, $1.1319\omega_m < \omega < 1.4\omega_m$), $0.5225\omega_m$ (COWP_N, $0.1949\omega_m < \omega < 0.7174\omega_m$) and $0.6638\omega_m$ (COWP_P, $0.7362\omega_m < \omega < 1.4\omega_m$). Moreover, we further calculated the corresponding group velocities (v_g) of the unidirectional modes in Figs. 4(b,e). As one can see, the EM signals in the COWP bands could propagate with $v_g > 0.05c$ (c is the light speed in vacuum). We note here that, due to the absence of the delay time and fan-in/fan-out[53], the information processing in the proposed device should be faster than in the electrical devices. In addition, the loss effect on the arms was also studied as the damping coefficient $\nu = 10^{-3}\omega$ as seen in Figs. 4(c) and 4(f). One can easily see the difference between the propagation lengths (L) in the upper and the lower COWP bands. More specifically, the EM waves in the COWP_P1 band in the arm

'A' could propagate about ten times longer than in the COWP_P2 band. Hence, the lower COWP band should be more suitable for the logic operations. According to our calculation, the unidirectional EM waves in the arm 'C' can always propagate with low loss ($L \geq 10^3$ mm). By far, we have studied the propagation characteristics, including the unidirectionality and low loss, in three arms of the basic Y-shaped module of the AODLS. In what follows, we will show how the one-way channels or the Y-shaped module can work as the LGs.

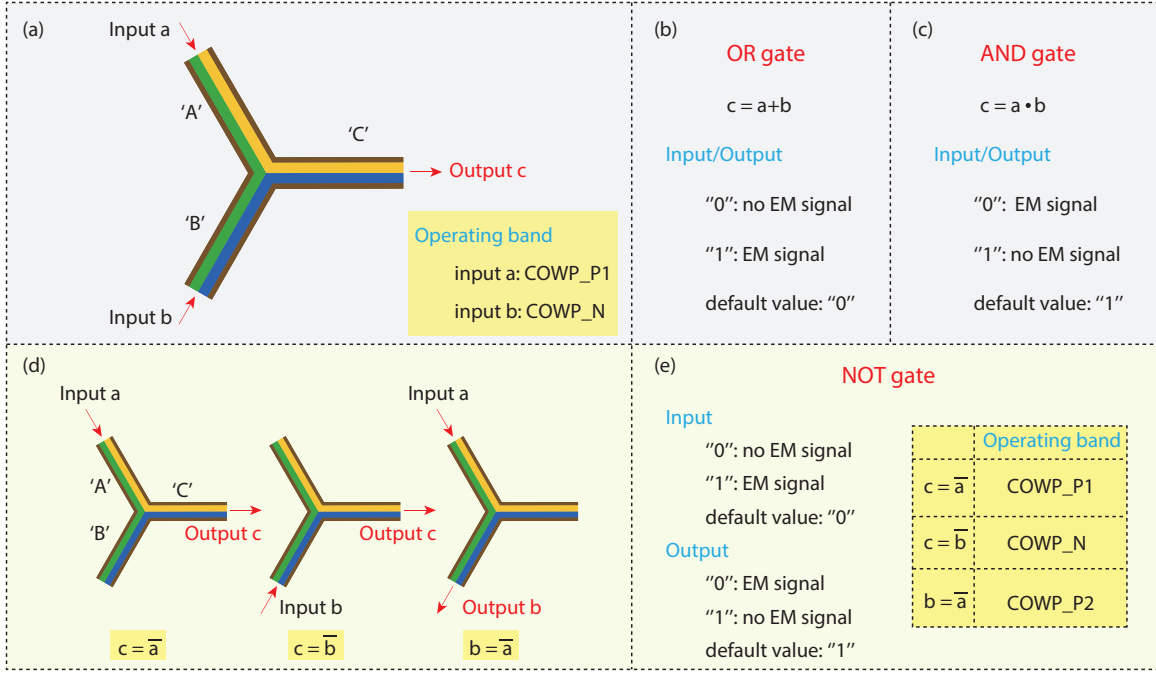


FIG. 5. Basic OR, AND, and NOT gates based on the Y-shaped module. (a) The schematic diagram of the OR and AND gates with two inputs and one output. (b) The schematic diagram of the NOT gates with one input and one output. (c)-(e) The theory of realization of the OR, AND, and NOT digital LGs.

III. REALIZATION OF THE BASIC LOGIC GATES

As we discussed above in the proposed Y-shaped structure in Fig. 4, the arms 'A' and 'C' can support unidirectionally forward propagating modes whereas the arm 'B' can only support backward modes. Here we consider the operating frequency within the region of $0.1949\omega_m < \omega < 0.7174\omega_m$ (see Fig. 4). In this condition, the launched one-way waves in arm 'A', due to the unidirectionality, could near-perfectly couple with the forward modes in arm 'C' and output in the end. Similar unidirectional signal transmission happens in the 'B'-'C' channel. Due to the two one-way channels, our proposed Y-shaped module can work as the OR and AND gate.

On the one hand, for the OR gate, we treat the existence of the EM signal in the arms as logic "1" while, on the contrary, the zero-energy state is regarded as logic "0" (see Fig. 5(b)). The default value/state in the OR gate is set to be logic "0". Relying on such a principle, any one of the input logic "1" (input unidirectional EM signal) will lead to the output logic "1" (output unidirectional EM signal), indicating the OR operation. On the other hand, the AND operation requires two input logic "1" to generate output logic "1". Nevertheless, the positive

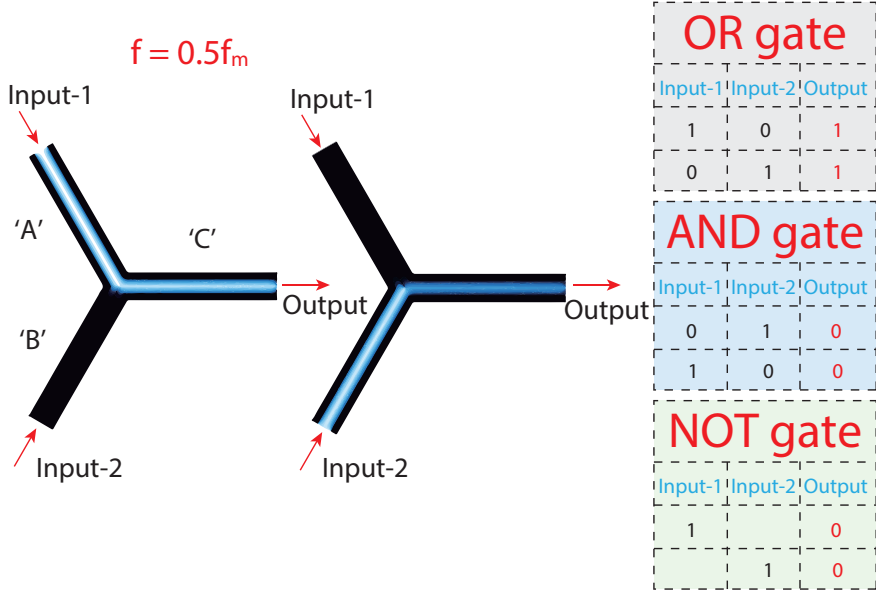


FIG. 6. Numerical simulations and the truth tables of the achievement of the OR, AND, and NOT gates in one shot.

logic used in the OR gate can not be used to achieve the AND gate. Here, we introduce the negative logic to achieve the AND gate based on the Y-shaped module. As contrasted with the OR gate, in the AND gate, we treat the EM propagation as logic "0" and treat no energy flow as logic "1", and set the default value to be logic "1" for both inputs and output (see Fig. 5(c)). In the AND gate, any one of the input EM waves (logic "0") will lead to output logic "0".

By utilizing the similar negative logic, the Y-shaped module can also serve as the NOT gate. As shown in Fig. 5(d), three channels of the proposed module can all work as the NOT gate, in which the EM energy represents logic "1" for the input arm and logic "0" (negative logic) for the output (see Fig. 5(e)). The input and output default values are logic "0" and logic "1", respectively. In this condition, the launched EM waves unidirectionally travel through the 'A'-'C', 'B'-'C', or 'A'-'B' channels, and meanwhile the input logic "1" turns to output logic "0", indicating the NOT operation. The colored panels in Figs. 5(a) and 5(e) demonstrate the operating bands of the inputs of the LGs. It is worth noting that in what follows, all the parameters of the Y-shaped module are the same as those in Fig. 4.

Different from the other optical LGs[9, 12, 13], our designed MO module can achieve multiple LGs functionalities in the same device without modifying. For instance, in Fig. 6, we performed two simulations in the Y-shaped module as $f = 0.5f_m$ by using the finite element method (FEM). In the first simulation (leftmost picture), the EM wave was excited in arm 'A' and as we expected, it traveled through the joint part and unidirectionally coupled into arm 'C'. In the next simulation, the EM wave with a backward propagation direction was launched in the arm 'B' and similarly, it propagated along the 'B'-'C' channel without backscattering. Accordingly, the input logic states in the first simulation are respectively ["]1", "0"] for the OR gate, ["]0", "1"] for the AND gate and ["]1", ""] for the NOT gate. On the contrary, the input logic states in the second simulation are respectively ["]0", "1"] for the OR gate, ["]1", "0"] for the AND gate, and [", "1"] for the NOT gate. Based on the proposed theory in Fig. 5, the output logic states in the

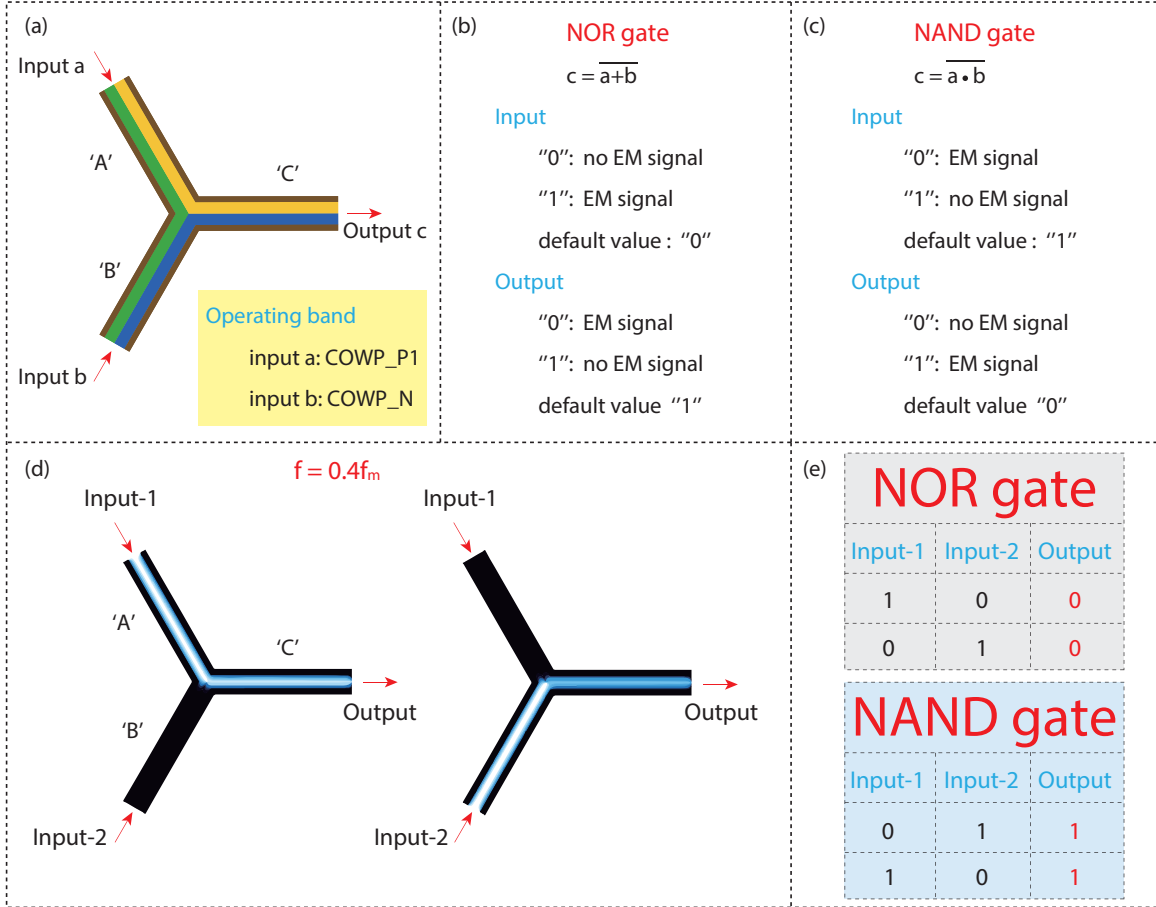


FIG. 7. (a) The schematic diagram of the NOR and NAND gates. (b,c) The theory of realization of the NOR and NAND gates. (d,e) Numerical simulations and the truth tables of the NOR and NAND gates.

two simulations are the same for both logic operations. The more clear results are exhibited in the rightmost truth tables. Due to the negative logic, the output logic states of the simulations are logic "0" in the AND and NOT operations while in the OR operation, the output read logic "1". Consequently, the Y-shaped module is capable of being used in multiple logic operations, and it is a multi-function LGs, which is potential for high-performance optical communication or calculation.

In addition, the Y-shaped module can also serve as the universal gates, i.e. the NOR and NAND gates. For the NOR operation, the principle is similar to that of the NOT gate except for the number of input signals. As shown in Fig. 7(a), because of the one-way characteristic, either input with logic "1" (EM signal) will lead to the output logic "0", implying the NOR operation. Moreover, the NAND gate can be achieved by thoroughly utilizing the negative logic in the NOR gate. In a word, completely replacing the logic states in the NOR gate to the opposite ones, i.e. "1" \rightarrow "0" and "0" \rightarrow "1" (see Figs. 7(b,c)). We further performed another two similar simulations like the ones in Fig. 6 to verify the NOR and NAND operations for a different working frequency $f = 0.4f_m$. As demonstrated in Figs. 7(d) and 7(e), the different inputs logic states will lead to output logic "0" for the NOR gate and logic "1" for the NAND gate. All the results of the simulations fit well with our theoretical analyses. Thus, we conclude here that our proposed Y-shaped module can not only work as the single basic LG, i.e. the OR,

AND, NOT, NOR, and NAND gates, but it can also work as a multiple outputs logical device. Besides, the XOR and XNOR gates could be easily achieved by comparing the EM energy intensity of the output and inputs of the Y-shaped configuration. For example, we could treat the existence of the output EM signal as logic "1" only if there is only one input EM signal, implying the XOR operation. One should also note that the logic states in our proposed LGs directly rely on the existence of the robust unidirectional EM signal, which is far more precise than the other proposed LGs. The proposed unidirectional modes-based logic LGs possess an extremely low error rate (E_r), extremely high contrast ratio (CR) and extinction ratio (ER), and super low signal-to-noise ratio because of the theoretically infinite intensity ratio of the logic states ("0" and "1") and robust one-way propagation property. Our designed LGs based on the one-way channels/modes can work in continuous and relatively broad COWP bands, which is another distinct feature of this kind of all-optical LGs.

IV. THE AODLS FOR MULTI-INPUT AND/OR MULTI-OUTPUT LOGIC OPERATIONS

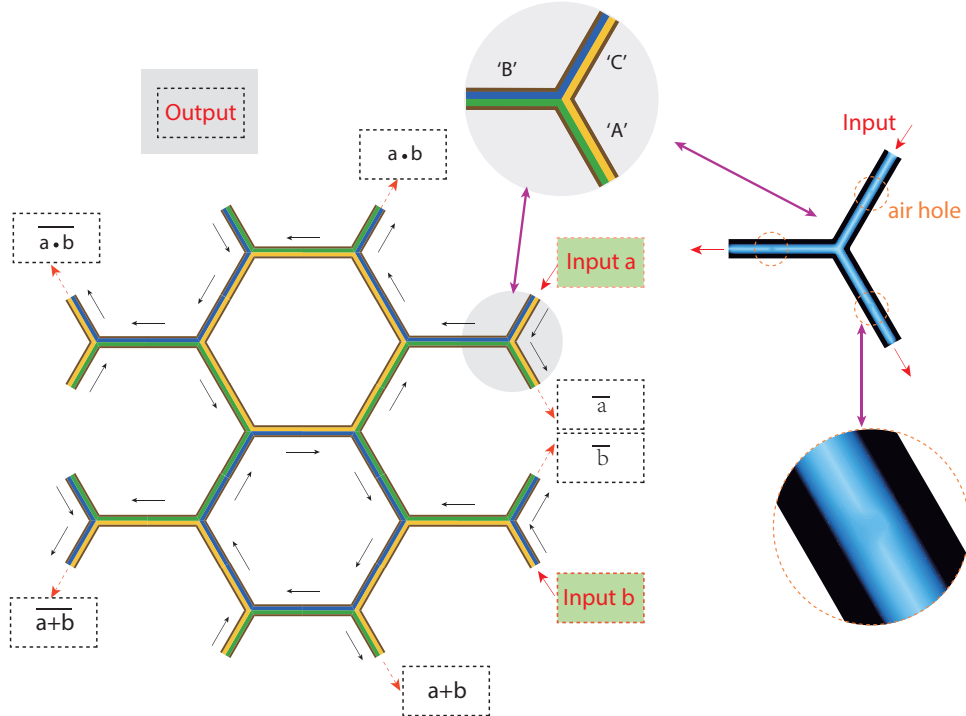


FIG. 8. Realization of multiport parallel logical computation system based on the Y-shaped module. The black arrows represent the path directions for the EM waves/signals.

The optical computation is characterized by the super-fast data transmission relying on the fan-in and fan-out[53], and our proposed unidirectional modes-based LGs have the continuous broad operating band. Moreover, since the basic LGs have been achieved by utilizing the Y-shaped module consisting of three YIG-based arms, in what follows, we will show how such a Y-shaped module could be used in designing the AODLS with the ability to expand to multi-input and/or -output optical logic system. The schematic of the AODLS is shown on the left side of Fig. 8. It needs to be emphasized that, in this subsection, we only consider the logic

operations in the lower COWP regions, i.e. $0.1948\omega_m < \omega < 0.7174\omega_m$. To clearly show the possible signal transmission, we added the black arrows in the schematic of the AODLS, which represent the propagation directions of the one-way channels. In the AODLS, six alternative outputs or logic operations can be chosen for two inputs. It is worth mentioning that the AODLS works with two inputs can be easily extended to the four-input logic device by suitably assembling the Y-shaped modules. Besides, the impinge part/module, as shown in the enlarged upper right picture in Fig. 8, is a left-hand connected 'A-B-C' module while the above Y-shaped module has a right-hand connection. In this incident module, the input EM waves from the arm 'C' can simultaneously transmit to the arms 'A' and 'B'. More clear results are displayed in the right diagrams, in which we injected an input EM signal with $f = 0.5f_m$, and three air holes with radius $r = 1\text{mm}$ were put on the YIG-YIG interfaces to further verify the robust unidirectionality of the incident EM modes. As one can see, the input EM wave perfectly bypassed the air hole in the arm 'C' and then split into two EM waves which still possess the robust one-way propagation characteristic. Thus, the incident module guarantees the NOT logic operation while part of the EM signal participates in other logic operations.

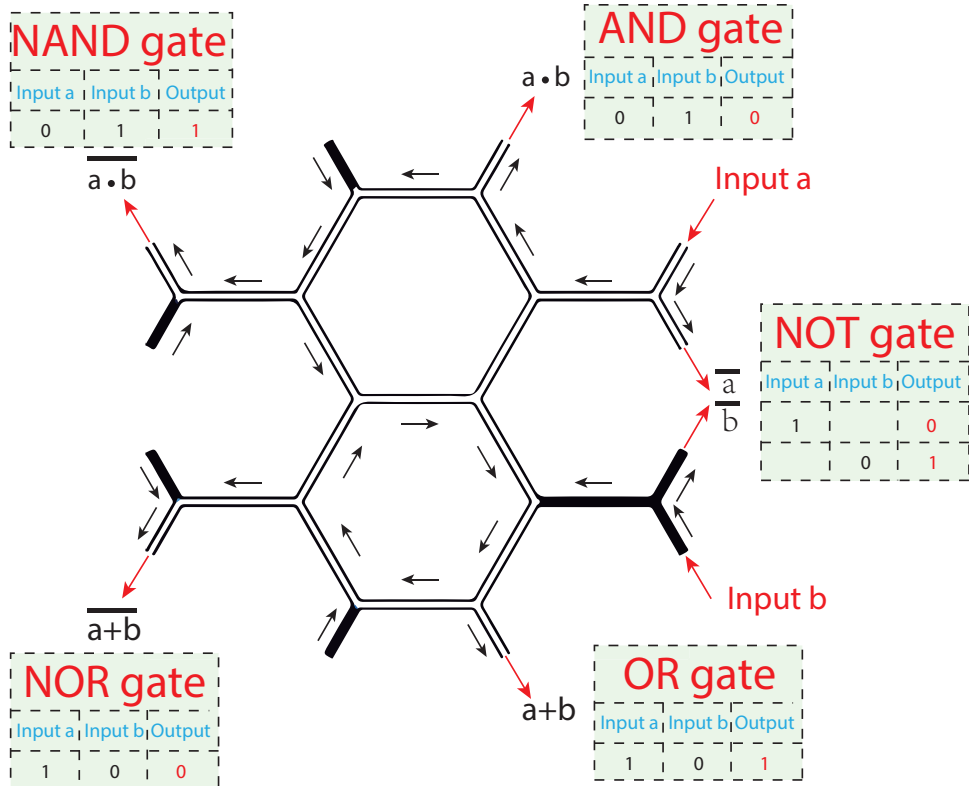


FIG. 9. Multi-output logic operation in the AODLS as the input EM wave with $f = 0.5f_m$.

In Fig. 9, we performed a FEM simulation in our designed AODLS. As expected, the input signal was unidirectionally transmitted along the one-way channels and exited via the outputs. Virtually no crosstalk or noise was observed during the logic operations, and the propagation characteristics of the EM wave are perfectly consistent with our theoretical analyses. More importantly, the proposed AODLS exhibits exotic multi-output logic operation with one-time input based on the robust unidirectional propagation of the EM signal(s). The OR, AND, NOT, NOR, and NAND gates were simultaneously achieved as demonstrated in the shaded truth tables in Fig. 9. Moreover, the AODLS has great potential for complex logic operations

due to its expansibility, precision, and broadband characteristic. Theoretically, no matter how complex the logic operation is, one can always achieve the specific logic operation by combining the unidirectional EM signal (logic "1" or "0") and the input-output intensities/phases. Furthermore, the unidirectional modes-based LGs, compared to the electrical ones, are more efficient since it is far easier to distinguish the existence of the EM signal(s) than to differentiate the relatively high and low levels.

V. CONCLUSION

In summary, we have proposed a novel all-optical digital logical system (AODLS) based on unidirectional modes. A basic Y-shaped module consisting of three YIG arms has been theoretically investigated. In the theoretical analysis, multiple complete one-way propagation (COWP) bands were found in the module, and intriguingly, the SMPs in the lower COWP band of the arm 'B' can only propagate in the opposite directions compared with the ones in other COWP bands. Relying on broadband one-way channels, and by utilizing the idea of negative logic, we have shown that the Y-shaped module can be used to achieve the OR, AND, NOT, NOR, and NAND gates independently or simultaneously. Possible realizations of the XOR and XNOR gates by comparing the input-output intensities have been proposed as well. Moreover, we have further designed the AODLS based on the Y-shaped configurations. By simply jointing the modules, we have achieved multi-output logic operations, which, to some degree, implies parallel computation. All logic operations are dependent on the existence of unidirectional EM signals, resulting in much more precise all-optical logic operations than the electrical ones, let alone the aspect of power loss. We emphasize that the proposed microwave AODLS could be extended to higher frequency bands once corresponding broadband unidirectional modes with opposite propagation directions are found and judiciously utilized [54]. Owing to the broad operating band, robust (one-way) signal transmission (huge signal-to-noise ratio), precision, composability, and extensibility, our proposed AODLS could be a novel platform for optical calculations and optical communication, and it is here believed that it has a great potential for designing integrated optical circuits.

ACKNOWLEDGEMENT

J. Xu and Y. Luo acknowledge the support of the Science and Technology Strategic Cooperation Programs of Luzhou Municipal People's Government and Southwest Medical University (2019LZXNYDJ18). J. Xu thanks the financial support from Funding of Southwest Medical University (20/00160222). F. Kang financially thanks for the support of the European Union's Horizon 2020 research and innovation program (H2020, no.713683) under the Marie Skłodowska-Curie grant agreement no. 713683 (COFUNDfellowsDTU), the Spring Buds Talent Program and its starting grant from Ningbo Institute of Materials Technology and Engineering (NIMTE) Chinese Academy of Sciences (CAS), and the "Double Hundred Talent" project and the starting grant from Sichuan University. K.L.T. was supported by the General Secretariat for Research and Technology (GSRT) and the Hellenic Foundation for Research and Innovation

- [1] Igor L. Markov. Limits on fundamental limits to computation. *Nature*, 512(7513):147–154, 2014.
- [2] He Yang, Vladislav Khayrulinov, Veer Dhaka, Hua Jiang, Anton Autere, Harri Lipsanen, Zhipei Sun, and Henri Jussila. Nanowire network-based multifunctional all-optical logic gates. *Science Advances*, 4(7):eaar7954, 2018.
- [3] James Hardy and Joseph Shamir. Optics inspired logic architecture. *Optics Express*, 15(1):150–165, 2007.
- [4] Stewart E Miller. Integrated optics: An introduction. *The Bell System Technical Journal*, 48(7):2059–2069, 1969.
- [5] Qianfan Xu and Michal Lipson. All-optical logic based on silicon micro-ring resonators. *Optics Express*, 15(3):924–929, 2007.
- [6] Akihiro Fushimi and Takasumi Tanabe. All-optical logic gate operating with single wavelength. *Optics Express*, 22(4):4466–4479, 2014.
- [7] Jayanta Kumar Rakshit and Jitendra Nath Roy. Micro-ring resonator based all-optical reconfigurable logic operations. *Optics Communications*, 321:38–46, 2014.
- [8] Ciyan Qiu, Weilu Gao, Richard Soref, Jacob T Robinson, and Qianfan Xu. Reconfigurable electro-optical directed-logic circuit using carrier-depletion micro-ring resonators. *Optics Letters*, 39(24):6767–6770, 2014.
- [9] Ying Zhang, Yongchang Lu, Mingrui Yuan, Yuehong Xu, Quan Xu, Quanlong Yang, Yingkai Liu, Jianqiang Gu, Yanfeng Li, Zhen Tian, Chunmei Ouyang, Weili Zhang, and Jiaguang Han. Rotated pillars for functional integrated on-chip terahertz spoof surface-plasmon-polariton devices. *Advanced Optical Materials*, 10(11):2102561, 2022.
- [10] Chinmoy Taraphdar, Tanay Chattopadhyay, and Jitendra Nath Roy. Mach-zehnder interferometer-based all-optical reversible logic gate. *Optics & Laser Technology*, 42(2):249–259, 2010.
- [11] Amer Kotb, Kyriakos E Zoiros, and Chunlei Guo. All-optical xor, nor, and nand logic functions with parallel semiconductor optical amplifier-based mach-zehnder interferometer modules. *Optics & Laser Technology*, 108:426–433, 2018.
- [12] Xiaoyu Yang, Xiaoyong Hu, Hong Yang, and Qihuang Gong. Ultracompact all-optical logic gates based on nonlinear plasmonic nanocavities. *Nanophotonics*, 6(1):365–376, 2017.
- [13] Yulan Fu, Xiaoyong Hu, Cuicui Lu, Song Yue, Hong Yang, and Qihuang Gong. All-optical logic gates based on nanoscale plasmonic slot waveguides. *Nano Letters*, 12(11):5784–5790, 2012.

- [14] Yungang Sang, Xiaojia Wu, Soniya S Raja, Chun-Yuan Wang, Haozhi Li, Yufeng Ding, Dahe Liu, Jing Zhou, Hyeyoung Ahn, Shangjr Gwo, et al. Broadband multifunctional plasmonic logic gates. *Advanced Optical Materials*, 6(13):1701368, 2018.
- [15] Hong Wei, Zhipeng Li, Xiaorui Tian, Zhuoxian Wang, Fengzi Cong, Ning Liu, Shunping Zhang, Peter Nordlander, Naomi J Halas, and Hongxing Xu. Quantum dot-based local field imaging reveals plasmon-based interferometric logic in silver nanowire networks. *Nano Letters*, 11(2):471–475, 2011.
- [16] Ye Liu, Fei Qin, Zi-Ming Meng, Fei Zhou, Qing-He Mao, and Zhi-Yuan Li. All-optical logic gates based on two-dimensional low-refractive-index nonlinear photonic crystal slabs. *Optics Express*, 19(3):1945–1953, 2011.
- [17] AG Coelho, MBC Costa, AC Ferreira, MG Da Silva, ML Lyra, and ASB Sombra. Realization of all-optical logic gates in a triangular triple-core photonic crystal fiber. *Journal of Lightwave Technology*, 31(5):731–739, 2012.
- [18] Yulan Fu, Xiaoyong Hu, and Qihuang Gong. Silicon photonic crystal all-optical logic gates. *Physics Letters A*, 377(3-4):329–333, 2013.
- [19] Yuhui Wang, Wenjing Liu, Zhurun Ji, Gaurav Modi, Minsoo Hwang, and Ritesh Agarwal. Coherent interactions in one-dimensional topological photonic systems and their applications in all-optical logic operation. *Nano Letters*, 20(12):8796–8802, 2020.
- [20] TK Paraïso, Michiel Wouters, Y Léger, F Morier-Genoud, and Benoit Deveaud-Plédran. Multistability of a coherent spin ensemble in a semiconductor microcavity. *Nature Materials*, 9(8):655–660, 2010.
- [21] Akihide Takeuchi, Hiroshi Yamagishi, Osamu Oki, Masakazu Morimoto, Masahiro Irie, and Yohei Yamamoto. Photochemically switchable interconnected microcavities for all-organic optical logic gate. *Advanced Functional Materials*, 31(34):2103685, 2021.
- [22] J Ding, Mikhail Kostylev, and AO Adeyeye. Realization of a mesoscopic reprogrammable magnetic logic based on a nanoscale reconfigurable magnonic crystal. *Applied Physics Letters*, 100(7):073114, 2012.
- [23] Weichao Yu, Jin Lan, Jiang Xiao, et al. Magnetic logic gate based on polarized spin waves. *Physical Review Applied*, 13(2):024055, 2020.
- [24] Roman Sordan, Floriano Traversi, and Valeria Russo. Logic gates with a single graphene transistor. *Applied Physics Letters*, 94(7):51, 2009.
- [25] Song-Lin Li, Hisao Miyazaki, Akichika Kumatori, Akinobu Kanda, and Kazuhito Tsukagoshi. Low operating bias and matched input- output characteristics in graphene logic inverters. *Nano Letters*, 10(7):2357–2362, 2010.

- [26] Young Tack Lee, Ji-Hoon Kang, Kisung Kwak, Jongtae Ahn, Hyun Tae Choi, Byeong-Kwon Ju, Seyed Hossein Shokouh, Seongil Im, Min-Chul Park, and Do Kyung Hwang. High-performance 2D MoS₂ phototransistor for photo logic gate and image sensor. *ACS Photonics*, 5(12):4745–4750, 2018.
- [27] Qijie Ma, Guanghui Ren, Kai Xu, and Jian Zhen Ou. Tunable optical properties of 2d materials and their applications. *Advanced Optical Materials*, 9(2):2001313, 2021.
- [28] Severin Daiss, Stefan Langenfeld, Stephan Welte, Emanuele Distante, Philip Thomas, Lukas Hartung, Olivier Morin, and Gerhard Rempe. A quantum-logic gate between distant quantum-network modules. *Science*, 371(6529):614–617, 2021.
- [29] Hyochul Kim, Ranojoy Bose, Thomas C Shen, Glenn S Solomon, and Edo Waks. A quantum logic gate between a solid-state quantum bit and a photon. *Nature Photonics*, 7(5):373–377, 2013.
- [30] Rami Barends, Alireza Shabani, Lucas Lamata, Julian Kelly, Antonio Mezzacapo, U Las Heras, Ryan Babbush, Austin G Fowler, Brooks Campbell, Yu Chen, et al. Digitized adiabatic quantum computing with a superconducting circuit. *Nature*, 534(7606):222–226, 2016.
- [31] Hong Wei, Zhuoxian Wang, Xiaorui Tian, Mikael Käll, and Hongxing Xu. Cascaded logic gates in nanophotonic plasmon networks. *Nature Communications*, 2:387, 2011.
- [32] Vilson R Almeida, Carlos A Barrios, Roberto R Panepucci, and Michal Lipson. All-optical control of light on a silicon chip. *Nature*, 431(7012):1081–1084, 2004.
- [33] Ye Chen, YinKe Cheng, RongBin Zhu, FeiFan Wang, HaoTian Cheng, ZhenHuan Liu, ChongXiao Fan, YuXuan Xue, ZhongCheng Yu, JianKun Zhu, et al. Nanoscale all-optical logic devices. *Science China Physics, Mechanics & Astronomy*, 62(4):1–15, 2019.
- [34] Jie Xu, Sanshui Xiao, Chiaho Wu, Hang Zhang, Xiaohua Deng, and Linfang Shen. Broadband one-way propagation and rainbow trapping of terahertz radiations. *Optics Express*, 27(8):10659–10669, 2019.
- [35] K. L. Tsakmakidis, L. Shen, S. A. Schulz, X. Zheng, J. Upham, X. Deng, H. Altug, A. F. Vakakis, and R. W. Boyd. Breaking lorentz reciprocity to overcome the time-bandwidth limit in physics and engineering. *Science*, 356(6344):1260–1264, 2017.
- [36] Jie Xu, Sanshui Xiao, Panpan He, Yazhou Wang, Yun Shen, Lujun Hong, Yamei Luo, and Bing He. Realization of broadband truly rainbow trapping in gradient-index metamaterials. *Optics Express*, 30(3):3941–3953, 2022.
- [37] S Ali Hassani Gangaraj, Boyuan Jin, Christos Argyropoulos, and Francesco Monticone. Broadband field enhancement and giant nonlinear effects in terminated unidirectional plasmonic waveguides. *Physical Review Applied*, 14(5):054061, 2020.

- [38] Francesco Monticone. A truly one-way lane for surface plasmon polaritons. *Nature Photonics*, 14(8):461–465, 2020.
- [39] Minkyung Kim, Wenlong Gao, Dasol Lee, Taewoo Ha, Teun-Teun Kim, Shuang Zhang, and Jun-suk Rho. Extremely broadband topological surface states in a photonic topological metamaterial. *Advanced Optical Materials*, 7(20):1900900, 2019.
- [40] Ling Lu, John D. Joannopoulos, and Marin Soljačić. Topological photonics. *Nature Photonics*, 8(11):821–829, 2014.
- [41] Mudi Wang, Ruo-Yang Zhang, Lei Zhang, Dongyang Wang, Qinghua Guo, Zhao-Qing Zhang, and Che Ting Chan. Topological one-way large-area waveguide states in magnetic photonic crystals. *Physical Review Letters*, 126(6):067401, 2021.
- [42] Z. Wang, Y. Chong, J. D. Joannopoulos, and M. Soljačić. Observation of unidirectional backscattering-immune topological electromagnetic states. *Nature*, 461(7265):772, 2009.
- [43] Kosmas L. Tsakmakidis, Christian Hermann, Andreas Klaedtke, Cécile Jamois, and Ortwin Hess. Surface plasmon polaritons in generalized slab heterostructures with negative permittivity and permeability. *Phys. Rev. B*, 73:085104, 2006.
- [44] Jie Xu, Qian Shen, Kai Yuan, Xiaohua Deng, Yun Shen, Hang Zhang, Chiaho Wu, Sanshui Xiao, and Linfang Shen. Trapping and releasing bidirectional rainbow at terahertz frequencies. *Optics Communications*, 473:125999, 2020.
- [45] Kosmas L. Tsakmakidis, Konstantinos Baskourellos, and Tomasz Stefański. Topological, nonreciprocal, and multiresonant slow light beyond the time-bandwidth limit. *Applied Physics Letters*, 119(19):190501, 2021.
- [46] Linfang Shen, Jie Xu, Yun You, Kai Yuan, and Xiaohua Deng. One-way electromagnetic mode guided by the mechanism of total internal reflection. *IEEE Photonics Technology Letters*, 30(2):133–136, 2017.
- [47] Zheng Wang, YD Chong, John D Joannopoulos, and Marin Soljačić. Reflection-free one-way edge modes in a gyromagnetic photonic crystal. *Physical Review Letters*, 100(1):013905, 2008.
- [48] Lei Bi, Juejun Hu, Peng Jiang, Dong Hun Kim, Gerald F Dionne, Lionel C Kimerling, and CA Ross. On-chip optical isolation in monolithically integrated non-reciprocal optical resonators. *Nature Photonics*, 5(12):758–762, 2011.
- [49] Joseph Shamir. Parallel optical logic operations on reversible networks. *Optics Communications*, 291:133–137, 2013.
- [50] Lujun Hong, Yazhou Wang, Yun Shen, Xiaohua Deng, Kai Yuan, Sanshui Xiao, and Jie Xu. Broadband energy squeezing and tunneling based on unidirectional modes. *Optical Materials Express*, 11(9):2975–2984, 2021.

- [51] Jie Xu, Xiaohua Deng, Hang Zhang, Chiaho Wu, Martijn Wubs, Sanshui Xiao, and Linfang Shen. Ultra-subwavelength focusing and giant magnetic-field enhancement in a low-loss one-way waveguide based on remanence. *Journal of Optics*, 22(2):025003, 2020.
- [52] David M Pozar. *Microwave Engineering*. John wiley & sons, 2011.
- [53] H John Caulfield and Shlomi Dolev. Why future supercomputing requires optics. *Nature Photonics*, 4(5):261–263, 2010.
- [54] Babak Bahari, Abdoulaye Ndao, Felipe Vallini, Abdelkrim El Amili, Yeshaiahu Fainman, and Boubacar Kanté. Nonreciprocal lasing in topological cavities of arbitrary geometries. *Science*, 358(6363):636–640, 2017.